# Sub-micron silicon nitride waveguide fabrication using conventional optical lithography

**Yuewang Huang, Qiancheng Zhao, Lobna Kamyab, Ali Rostami, Filippo Capolino and Ozdal Boyraz***

*EECS Department, University of California, Irvine, California 92697, USA*
*oboyraz@uci.edu

**Abstract:** We demonstrate a novel technique to fabricate sub-micron silicon nitride waveguides using conventional contact lithography with MEMS-grade photomasks. Potassium hydroxide anisotropic etching of silicon facilitates line reduction and roughness smoothing and is key to the technique. The fabricated waveguides is measured to have a propagation loss of 0.8dB/cm and nonlinear coefficient of $\gamma$ = 0.3/W/m. A low anomalous dispersion of <100ps/nm/km is also predicted. This type of waveguide is highly suitable for nonlinear optics. The channels naturally formed on top of the waveguide also make it promising for plasmonics and quantum efficiency enhancement in sensing applications.

©2015 Optical Society of America

**OCIS codes:** (130.2790) Guided waves; (220.3740) Lithography; (230.7370) Waveguides.

## References and links

1. G. T. Reed, *Silicon Photonics: The State of the Art* (Wiley-Interscience, 2008).
2. L. Vivien and L. Pavesi, *Handbook of Silicon Photonics* (Taylor & Francis, 2013).
3. W. Bogaerts, R. Baets, P. Dumon, V. Wiaux, S. Beckx, D. Taillaert, B. Luyssaert, J. Van Campenhout, P. Bienstman, and D. Van Thourhout, "Nanophotonic waveguides in silicon-on-insulator fabricated with CMOS technology," J. Lightwave Technol. **23**(1), 401–412 (2005).
4. R. Soref, "The past, present, and future of silicon photonics," IEEE J. Sel. Top. Quantum Electron. **12**(6), 1678–1687 (2006).
5. D. D. John, M. J. R. Heck, J. F. Bauters, R. Moreira, J. S. Barton, J. E. Bowers, and D. J. Blumenthal, "Multilayer Platform for Ultra-Low-Loss Waveguide Applications," IEEE Photon. Technol. Lett. **24**(11), 876–878 (2012).
6. D. J. Moss, R. Morandotti, A. L. Gaeta, and M. Lipson, "New CMOS-compatible platforms based on silicon nitride and Hydex for nonlinear optics," Nat. Photonics **7**(8), 597–607 (2013).
7. S. Romero-García, F. Merget, F. Zhong, H. Finkelstein, and J. Witzens, "Silicon nitride CMOS-compatible platform for integrated photonics applications at visible wavelengths," Opt. Express **21**(12), 14036–14046 (2013).
8. J. S. Levy, A. Gondarenko, M. A. Foster, A. C. Turner-Foster, A. L. Gaeta, and M. Lipson, "CMOS-compatible multiple-wavelength oscillator for on-chip optical interconnects," Nat. Photonics **4**(1), 37–40 (2010).
9. K. Ikeda, R. E. Saperstein, N. Alic, and Y. Fainman, "Thermal and Kerr nonlinear properties of plasma-deposited silicon nitride/ silicon dioxide waveguides," Opt. Express **16**(17), 12987–12994 (2008).
10. S. Minissale, S. Yerci, and L. D. Negro, "Nonlinear optical properties of low temperature annealed silicon-rich oxide and silicon-rich nitride materials for silicon photonics," Appl. Phys. Lett. **100**(2), 021109 (2012).
11. Y. Huang, Q. Zhao, L. Kamyab, A. Rostami, F. Capolino, and O. Boyraz, "Sub-micron silicon nitride waveguide fabrication using conventional optical lithography," in *Advanced Photonics for Communications*, OSA Technical Digest (online) (Optical Society of America, 2014), p. JT3A.27.
12. H. Seidel, L. Csepregi, A. Heuberger, and H. Baumgärtel, "Anisotropic Etching of Crystalline Silicon in Alkaline Solutions," J. Electrochem. Soc. **137**(11), 3626–3632 (1990).
13. B. Kloeck, S. D. Collins, N. F. de Rooij, and R. L. Smith, "Study of electrochemical etch-stop for high-precision thickness control of silicon membranes," IEEE Trans. Electron. Dev. **36**(4), 663–669 (1989).
14. C. H. Henry, R. F. Kazarinov, H. J. Lee, K. J. Orlowsky, and L. E. Katz, "Low loss Si3N4-SiO2 optical waveguides on Si," Appl. Opt. **26**(13), 2621–2624 (1987).
15. J. F. Bauters, M. J. R. Heck, D. John, D. Dai, M.-C. Tien, J. S. Barton, A. Leinse, R. G. Heideman, D. J. Blumenthal, and J. E. Bowers, "Ultra-low-loss high-aspect-ratio Si3N4 waveguides," Opt. Express **19**(4), 3163–3174 (2011).
16. F. P. Payne and J. P. R. Lacey, "A theoretical analysis of scattering loss from planar optical waveguides," Opt. Quantum Electron. **26**(10), 977–986 (1994).

#230992 - $15.00 USD Received 17 Dec 2014; revised 22 Feb 2015; accepted 26 Feb 2015; published 4 Mar 2015

17. K. Wörhoff, A. Driessen, P. V. Lambeck, L. T. H. Hilderink, P. W. C. Linders, and T. J. A. Popma, “Plasma enhanced chemical vapor deposition silicon oxynitride optimized for application in integrated optics,” Sens. Actuat. Phys. **74**(1-3), 9–12 (1999).
18. N. Daldosso, M. Melchiorri, F. Riboli, F. Sbrana, L. Pavesi, G. Pucker, C. Kompocholis, M. Crivellari, P. Bellutti, and A. Lui, “Fabrication and optical characterization of thin two-dimensional Si3N4 waveguides,” Mater. Sci. Semicond. Process. **7**(4-6), 453–458 (2004).
19. M. Melchiorri, N. Daldosso, F. Sbrana, L. Pavesi, G. Pucker, C. Kompocholis, P. Bellutti, and A. Lui, “Propagation losses of silicon nitride waveguides in the near-infrared range,” Appl. Phys. Lett. **86**(12), 121111 (2005).
20. A. Melloni, F. Morichetti, R. Costa, G. Cusmai, R. G. Heideman, R. Mateman, D. H. Geuzebroek, and A. Borreman, “TriPleX: A new concept in optical waveguiding,” in *13th Eur. Conf. Integrated Optics (ECIO),* Copenhagen, Denmark (2007).
21. K. Ikeda, R. E. Saperstein, N. Alic, and Y. Fainman, “Thermal and Kerr nonlinear properties of plasma-deposited silicon nitride/ silicon dioxide waveguides,” Opt. Express **16**(17), 12987–12994 (2008).
22. J. S. Levy, A. Gondarenko, M. A. Foster, A. C. Turner-Foster, A. L. Gaeta, and M. Lipson, “CMOS-compatible multiple-wavelength oscillator for on-chip optical interconnects,” Nat. Photonics **4**(1), 37–40 (2010).
23. C.-Y. Tai, J. S. Wilkinson, N. M. Perney, M. C. Netti, and J. J. Baumberg, “Self-phase modulation induced spectral broadening of ultrashort laser pulses in tantalum pentoxide (Ta) rib waveguide, ” in The 5th Pacific Rim Conference on Lasers and Electro-optics (CLEO) (2003).
24. J. Levy, “Integrated Nonlinear Optics In Silicon Nitride Waveguides And Resonators,” Ph.D. dissertation, Cornell Univ. (2011).
25. P. N. Kean, K. Smith, and W. Sibbett, “Spectral and temporal investigation of self-phase modulation and stimulated Raman scattering in a single-mode optical fibre,” Optoelectron. IEE Proc. J **134**, 163–170 (1987).
26. R. A. Soref, J. Schmidtchen, and K. Petermann, “LARGE SINGLE-MODE RIB WAVE-GUIDES IN GESI-SI AND SI-ON-SIO2,” IEEE J. Quantum Electron. **27**(8), 1971–1974 (1991).
27. Y. Huang, S. K. Kalyoncu, Q. Zhao, R. Torun, and O. Boyraz, “Silicon-on-sapphire waveguides design for mid-IR evanescent field absorption gas sensors,” Opt. Commun. **313**, 186–194 (2014).
28. G. P. Agrawal, *Nonlinear Fiber Optics, Fifth Edition* (Academic Press, 2013).

## 1. Introduction

Under the drive of optoelectronic integration, silicon photonics have seen huge development and booming in the past decades. A wide range of optoelectronic devices ranging from modulators to lasers based on silicon have become available in CMOS-compatible foundry fabrication process [1,2]. As the most fundamental building block, silicon waveguides have been maturated in integrated process lines with ultra-low propagation loss [3,4]. These waveguides are all based on silicon-on-insulator (SOI) technology. As the waveguide dimension shrinks, thicker buried oxide (BOX) layer is necessary to prevent leakage to the silicon substrate, which is in contrary to the tendency of thinner oxide layer in CMOS electronics. Expensive SOI wafers with thick BOX have to be used as the starting substrate of the fabrication process. Recently, the waveguide platform based on silicon nitride ($Si_3N_4$) has emerged as an alternative to SOI silicon platform for integrated photonic circuit [5–7]. Compared to silicon waveguide built on top of expensive SOI wafers, $Si_3N_4$ waveguides can be built on bulk silicon substrates at relatively low cost. Both the oxide buffer layer (i.e., $SiO_2$) and the guiding material (i.e., $Si_3N_4$) can be easily deposited in standard CMOS lines using plasma-enhanced vapor deposition (PECVD) or low pressure vapor deposition (LPCVD) on silicon wafers at very low cost. Another advantage of $Si_3N_4$ waveguide over Si waveguide is the absence of two-photon-absorption and free-carrier-absorption which deteriorate propagation loss and high power nonlinear applications [8]. Low propagation loss at both visible and near infrared has been achieved in both PECVD and LPCVD deposited $Si_3N_4$ waveguides [9,10]. These low loss waveguides are of relatively large dimensions and defined by high resolution lithography using E-beam or stepper. It is very attractive if the highly accessible UV contact lithography can be accommodated to fabricate low loss waveguides [11]. However, the resolution limit of direct contact lithography is larger than 1μm due to optical diffraction limit. Even for large waveguides with dimension greater than 1μm, high quality photomasks with smooth edges are still necessary in order to deliver low loss waveguides. In this report, we present such a fabrication technique that enables fabrication of sub-micron $Si_3N_4$ waveguides using *i*-line UV contact lithography with very

#230992 - $15.00 USD Received 17 Dec 2014; revised 22 Feb 2015; accepted 26 Feb 2015; published 4 Mar 2015
© 2015 OSA

low cost MEMS grade photomasks. While our preliminary result has been presented in earlier conference [11], here we report the details of waveguide fabrication, nonlinearity measurement and dispersion calculations. We show that a sequence of photolithography steps followed by KOH wet etching, thermal oxidation, and LPCVD $Si_3N_4$ deposition can produce sub-micron trench line waveguides with low loss and suitable for microfluidic sensing and nonlinear optical applications. The guiding material is deposited in the etched trenches to form the $Si_3N_4$ waveguides. The process is also CMOS compatible. With this technique, we successfully fabricated $Si_3N_4$ waveguide with a width of 0.8 μm and effective mode area of $A_{eff}$ = 1.9 μm$^2$. We achieved a low propagation loss of 0.8 ± 0.26 dB/cm. We also measured the nonlinear refractive index of the deposited $Si_3N_4$ film to be $n_2 = 1.39 \times 10^{-19}$ m$^2$/W (i.e., $\gamma = 0.3W^{-1}/m$) and low anomalous dispersion of <100ps/nm/km in telecommunication window.

## 2. Waveguides fabrication: line reduction and roughness smoothing

In order to fabricate sub-micron waveguide by using conventional optical lithography, there are two major challenges. First, the resolution of contact lithography is >1μm and special photo resist and high quality masks have to be used in order to get close to this limit. Also, MEMS grade masks often have a large critical dimension and direct patterning will result in a wide waveguide supporting multiple modes. Hence a linewidth reduction mechanism has to be established. Second, due to limited resolution, features on these photomasks tend to have rough edges as shown in Fig. 1(b). This would lead to formidable scattering loss when used to directly pattern optical waveguide. Special methods have to be adopted to smooth the edge roughness. In our fabrication, these two mechanisms are achieved by utilizing the anisotropic KOH etching and thermal oxidation. The fabrication process is shown in Fig. 1. A layer of 500 nm $SiO_2$ and 1.2μm PR are first deposited and coated on the substrate. The PR layer is patterned with contact UV photo-lithography by using a low-cost MEMS grade photomask consisting of straight line openings with a critical dimension (CD) of 4 μm. The PR is developed later on to form large line openings of $W_{top}$ to feature the photomask pattern after UV exposure at 365 nm. Afterwards, the pattern is transferred to the oxide layer by ICP etching to form a hard mask for the following KOH etching. The KOH recipe etches the silicon substrate along the <100> direction for a depth of $H_{Si}$. Since the KOH silicon etching is highly anisotropic and etching rate along <111> direction is extremely slow, the wet etching will essentially stop at the (111) plane and trapezoidal or triangular shape trenches will be formed as shown in the 6th diagram in Fig. 1. The slope follows the (111) plane and forms an angle of $\tan^{-1}\sqrt{2} = 54.7°$ As a result, V-grooves will be etched if the linewidth ($W_{top}$) on the photomask is smaller than $2\times\sqrt{2}/2\times H_{Si}$. On the other hand, if the original linewidth is larger than that amount, the KOH etching will create an inverted isosceles trapezoidal shape with the lower edge $2\times\sqrt{2}/2\times H_{Si}$ smaller than the upper edge, which equals the linewdith on the photomask. For example, if the linewidth of the openings on the photomask is 5 μm, the lower edge of the etched trenches will be only $W_{btm} = 5 - 2\times\sqrt{2}/2\times 3 = 0.8\mu m$ given a Si etching depth of 3μm. For the proof of concept fabrication efforts demonstrated here, we used timed etching and aqueous alkaline concentration to control the etching depth. The total etch time of 10 min allows us to achieve waveguide dimensions with 100 nm precision in a standard clean room environment. If further precision is required, a highly doped boron-silicon layer [12] should be inserted or p-n junction layer [13] should be added as etch stopper to achieve desired precision. Sub-micron waveguide width is achieved by using this line reduction technique based on KOH etching. As a result, since the only process that requires human involvement that is prone to error is the KOH etching that essentially stops at the (111) crystalline plane and is highly reproducible considering the precision of Si crystal structure for proposed geometries. In fact, the fabrication steps performed in this work are as_reproducible as most dry etching methods.

#230992 - $15.00 USD Received 17 Dec 2014; revised 22 Feb 2015; accepted 26 Feb 2015; published 4 Mar 2015
© 2015 OSA

Moreover, KOH wet etching also dramatically smoothens the line edges. Despite the coarse mask, KOH etching eliminates the surface roughness as shown by SEM images taken during the development phase in Fig. 1(e). Figure 1(b)-(d) shows the effect of roughness smoothing in the KOH etching. The line edges after the KOH etching in Fig. 1(d) are dramatically smoothened compared to the patterns on the Fig. 1(b) photomask and 1(c) PR layer. After removing oxide hard mask, a layer of 3µm thermal oxide is grown to serve as a buffer layer to isolate the optical field from leaking into the silicon substrate. Thermal oxidation also helps on roughness smoothing to a further extent. Hereafter, a nitride layer of 725 nm was deposited on the sample and in the oxidized trenches using LPCVD. This concludes the silicon nitride waveguide fabrication and the optical wave will be guided in the nitride in the valley of the trenches.

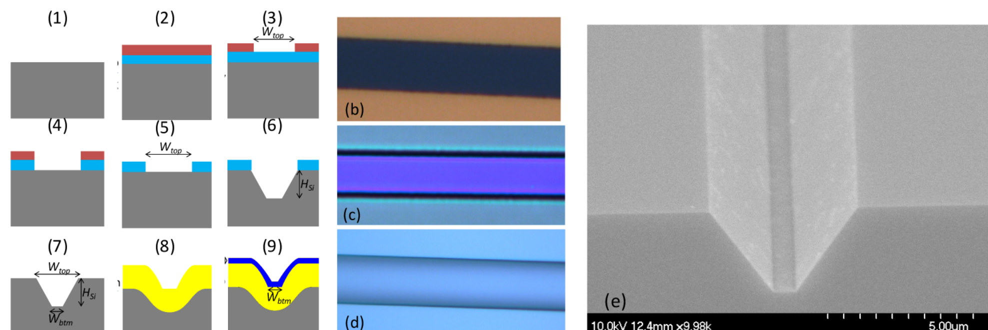


Fig. 1. Fabrication process flow. A final annealing step is not shown in the figure. Roughness smoothing by KOH wet etching. (b) Optical microscope graph of the photomask with 5 µm linewidth: edge roughness is observable; (c) optical microscope graph of the PR pattern: the edge roughness is transferred to the PR pattern; (d)Optical microscope graph of the pattern after KOH etching: the edges are dramatically smoothened. (e) KOH etching eliminates the surface roughness generated by coarse MEMS grade photomask.

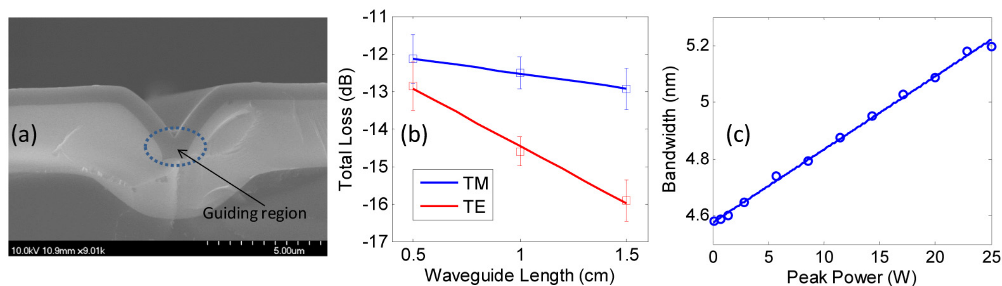


Fig. 2. (a) SEM of the fabricated waveguide. (b) Total loss of waveguide with different length using cut-back method. (c) SPM broadening at different input peak power levels. A nonlinear refractive index of $n_2 = 1.39 \times 10^{-19} \mathrm{m}^2/\mathrm{W}$ was derived from the curve.

## 3. Waveguide experimental characterization

Figure 2(a) shows the SEM images of the fabricated waveguide with $W_{top}$ = 5 µm. The guiding region is circled out in the SEM. The effective dimension of the waveguide is approximately $W_{btm} \times H_{Si3N4} \approx 0.8$ µm × 0.9 µm. After the waveguide fabrication, we diced the waveguides and polished the waveguide ends with lapping films for optical quality facets (<0.1 µm grain size). We then characterized the waveguide loss using the cut-back method. As shown in Fig. 2(b), we measure the total loss of the waveguides with three different lengths: $L$ = 0.5 cm, 1 cm and 1.5 cm respectively. From the slope, we derived a waveguide propagation loss of 0.8 ± 0.26 dB/cm for TM mode. As expected, the fabricated waveguides are polarization sensitive and TE mode has higher propagation loss of 3.13 ± 0.37 dB/cm.

#230992 - $15.00 USD Received 17 Dec 2014; revised 22 Feb 2015; accepted 26 Feb 2015; published 4 Mar 2015
© 2015 OSA

Unlike high aspect ratio waveguides in which most of the mode energy propagates in the cladding region [14,15], the mode of the waveguides reported here is tightly confined in the waveguide core region, and hence, makes modes more susceptible to losses induced by surface roughness [16] at the top layer. See Table 1. An oxide cap layer to passivate the waveguide surface can reduce the propagation loss. Since these waveguides are designed for sensory applications, oxide cap layer has not been deposited intentionally. The second reason for reported losses arises from the mode leakage to slab region. This can be minimized by increasing the etch depth of trenches. Moreover, the waveguide loss can be further reduced by using stoichiometric nitride which is known to be more transparent than silicon rich nitride [15] and optimizing the post annealing temperature and time to reduce the Si-H and N-H absorption [17]. We used a tapered lens fiber for butt-coupling, and the estimated insertion loss is ~8 dB without any optimization. Bending losses has not been studied at this stage it will be part of elaborate 3D numerical study we are working on.

**Table 1. Comparison between our work and previous publications**

| Waveguide dimension (silicon nitride region) | Propagation loss | Wavelength | Year |
|---|---|---|---|
| w≈0.8 μm,h = 0.9 μm | 0.8 ± 0.26 dB/cm | 1550 nm | Our work |
| w = 4 μm, h = 0.12 μm | 0.3 dB/cm | 1.3-1.6 μm | 1987 [14] |
| w = 12.8 μm, h = 200 nm | 4.8 ± 0.5dB/cm | 1544 nm | 2004 [18] |
| w >10 μm, h = 500 nm multilayer | 1.5 ± 0.2 dB/cm | 1550 nm | 2005 [19] |
| w = h ≈1.1 μm | 0.06~0.08 dB/cm | 1460-1530 nm | 2007 [20] |
| w = 1 μm, h = 0.5 μm | ~4 dB/cm | 1550 nm | 2008 [21] |
| w = 1.45 μm, h = 725 nm, 23° wall angle | 0.5 dB/cm | 1550 nm | 2010 [22] |
| w = 2.8 μm, h = 80 nm, 2 mm bending radius | 0.03 dB/cm | 1550 nm | 2011 [15] |

To possibly facilitate nonlinear applications in these waveguides, we also want to characterize the nonlinear property of the waveguides. Particularly we pursued the nonlinear refractive index, $n_2$, of the silicon nitride, which is related with the third order susceptibility of $Si_3N_4$. Here, we measured the nonlinear refractive index by utilizing the spectral broadening caused by self-phase-modulation (SPM) of high energy pulses in nonlinear medium [23,24]. According to [23,25],under the Gaussian beam excitation assumption, the spectral broadening caused by SPM can be theoretically expressed as

$$\Delta\lambda = \Delta\lambda_i + 4\sqrt{\frac{2\ln 2}{e}} \cdot \frac{\lambda_0 n_2 L_{eff}}{cA_{eff}} \frac{P}{t_p} \tag{1}$$

Here, $\Delta\lambda_i$ is the bandwidth of the input laser pulse, $\lambda_0$ is the center wavelength, $n_2$ is the nonlinear refractive index, $L_{eff}$ is the effective length defined by $L_{eff} = \left(1-\exp(-\alpha L)\right)/\alpha$ with $\alpha$ being waveguide loss coefficient and $L$ being waveguide length, $A_{eff}$ is the effective mode area, $P$ is the peak pulse power and $t_p$ is the full-width-at-half-maximum (FWHM) pulse width. According to Eq. (1), the spectral broadening caused by SPM is linearly related to the pulse peak power and the slope coefficient is also linearly related with the nonlinear refractive index $n_2$. If we can determine the spectral broadening for different input power levels, we can derive the nonlinear refractive index from the slope coefficient of the curve. To accomplish this, we coupled high power optical pulses into the 1.5 cm $Si_3N_4$ waveguides and measured the 3 dB bandwidth of the output pulses. Figure 2(c) shows the 3 dB bandwidth of the femtosecond laser pulse at waveguide output with different input peak power. With the propagation loss of 0.8 dB/cm from loss measurement and an effective mode area of $A_{eff}$ = 1.9 $\mu m^2$, we estimated a nonlinear refractive index value of $n_2 = 1.39 \times 10^{-19}$ $m^2/W$ from the slope of the fitted linear curve. This value agrees well with the values reported in other literatures [9,24]. This corresponds to a nonlinear parameter of $\gamma = \left(\omega n_2\right)/\left(cA_{eff}\right) = 0.3W^{-1}/m$ for the

#230992 - $15.00 USD Received 17 Dec 2014; revised 22 Feb 2015; accepted 26 Feb 2015; published 4 Mar 2015
© 2015 OSA

waveguide, which is >100 times larger than that in single-mode fibers. It is worth noting that the effective mode area $A_{eff}$ varies for difference waveguides because the irregular shapes. Higher nonlinearity applications may seek the trench waveguides with small effective mode areas and low propagation loss properties. In a word, the $Si_3N_4$ waveguides are suitable for nonlinear applications based on third order nonlinearity.

## 4. Waveguide numerical characterization

We also put these structures defined by SEM images into a finite-element solver (COMSOL MultiPhysics) to further investigate the properties of the waveguides. In the simulation, the refractive index of the $Si_3N_4$ film was measured using ellipsometry and modeled by Sellmeire equation as $n^2 = 1 + 3.585\lambda^2 / (\lambda^2 - 0.1316^2)$, where $\lambda$ is in the unit of μm. One can assume the waveguide shown in Fig. 2(a) to be a rib waveguide with width of 0.8 μm, height of 0.9 μm and out-inner ratio $r$ of 0.725/0.9 = 0.806 approximately. Thereby single-mode conditions for rib waveguide can be used as approximate design approach before extensive numerical simulations [26]. Considering the bends of the silicon nitride waveguide, the single-mode condition may be even loose for trench waveguides than for the planar rib waveguides. The aforementioned waveguide can only support TE and TM fundamental modes. Figure 3(a) and 3(b) shows the simulated mode profile of the fundamental TM and TE mode of the waveguides. The mode profiles are of heart shape. The TE mode shows strong field enhancement at waveguide surface. This is desirable for sensing and nonlinear excitation of deposited nanoparticles applications. However, the propagation loss is expected be higher. This also agrees with the propagation loss measurements in the previous section. The TM mode is more concentrated in the $Si_3N_4$ than TE mode, which leads to a higher effective index in the TM mode as shown in Fig. 3(c). However, the effective mode area of TM mode is large than TE mode as shown in Fig. 3(d). The effective mode area is ~1.9 μm$^2$ and ~1.55 μm$^2$ for TM and TE mode. Figure 3(e) shows the evanescent power ratio (ERP), defined as the ratio of the evanescent field power in the air trench with respect to the total modal power [27]. ERP values of >2% is predicted for the designed $Si_3N_4$ waveguide with $T_{Si3N4}$ = 0.725 μm. This type of waveguide can be designed to have stronger evanescent field in the air trenches by using a thinner $Si_3N_4$ thickness, e.g. ~10% for $T_{Si3N4}$ = 0.25 μm. A large EPR is highly desirable for enhanced interaction with micro fluid or plasmonic coating in sensing applications [27]. Figure 3(f) shows the calculated dispersion of the silicon nitride waveguide. Both the TM and TE mode are in the anomalous dispersion region and very small dispersion values, <100ps/nm.km, are expected in these waveguides in the telecommunication window, which makes them very promising for nonlinear parametric process requiring phase matching, e.g. four-wave-mixing (FWM) applications [28]. The TM mode shows lower dispersion than TE mode.

#230992 - $15.00 USD Received 17 Dec 2014; revised 22 Feb 2015; accepted 26 Feb 2015; published 4 Mar 2015
© 2015 OSA

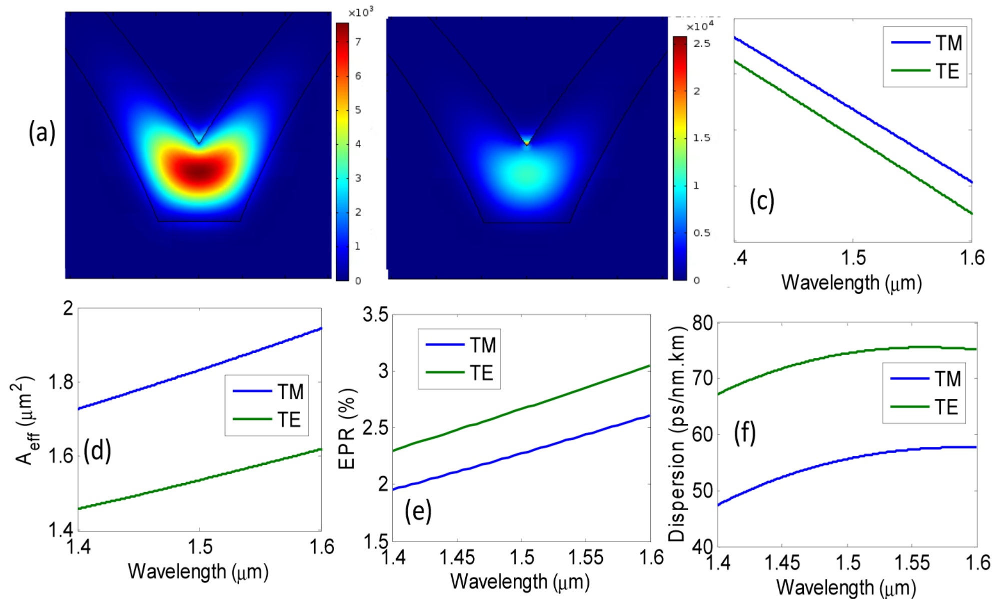


Fig. 3. Numerical simulation results for the waveguide: (a)TM mode profile ($|E_y|^2$); (b) TE mode profile($|E_x|^2$); (c) effective mode index; (d) effective mode area; (e) evanescent power ratio; and (f) GVD dispersion of the $Si_3N_4$ waveguide for different wavelengths.

## 5. Summary

In summary, we proposed a CMOS-compatible technique to fabricate sub-micron silicon nitride waveguide on Si substrate using conventional contact optical lithography. With this technique, requirements on photomasks are largely relaxed and even low cost MEMS grade photomask with high CD > 4 µm is adequate to produce waveguides with propagation loss less than 1 dB/cm. The power of the technique lies in the line reduction and roughness smoothing coming along with the KOH wet etching of silicon. Large openings on the top of the valley will be reduced to trenches of sub-micron dimension at the bottom. The wet etching process also drastically smoothes the roughness on the patterns defined by lithography. After thermal oxidation, silicon nitride film is deposited in the trenches to form the final $Si_3N_4$ waveguide. The fabricated waveguide has an effective dimension of ~0.8µm × 0.9µm. We measured a propagation loss as low as 0.8 ± 0.26 dB/cm. The loss can potentially be further reduced by increasing the etching depth or using stoichiometric nitride with multiple temperature cycling [15]. We also measured a nonlinear refractive index value of $n_2 = 1.39 \times 10^{-19}$ m$^2$/W, corresponding to a nonlinear parameter of $\gamma = 0.3$ W$^{-1}$/m . The losses can further optimized with optimized deposition rates and post annealing process. Also, simulation also shows low dispersion of <100ps/nm.km in the anomalous region that can be used for parametric process. The combination makes the $Si_3N_4$ waveguides highly suitable for nonlinear applications based on the parametric process relying on phase matching. Another interesting merit of the process is the channels right above the waveguides, which can be used as micro fludic channels for evanescent field based sensing applications [27]. We are also exploring deposition of nano-particles and quantum dots in the channels for plasmonic and quantum efficiency enhancement. Meanwhile, waveguides with BOX layer using chemical deposition method are also under pursuit.

### Acknowledgments

This research was partially supported by the National Science Foundation (NSF) Award No. ECCS-1028727 and ECCS-1449397.